Available online at BCREC website: https://bcrec.id

Bulletin of Chemical Reaction Engineering & Catalysis, 17 (2) 2022, 331-339

Research Article

Effect of pH on the Performance of $Bi_2O_2CO_3$ Nanoplates for Methylene Blue Removal in Water by Adsorption and Photocatalysis

Trung Thanh Nguyen[1,2,*], Tri Thich Le[1,2], Thi Bao Tran Nguyen[1,2], Thuy Nguyen Thi[2,3], Le Ba Tran[1,2,3], Thi Quynh Anh Nguyen[1,2], Nhat Huy Nguyen[2,4,*]

[1]Laboratory of Nanomaterial, An Giang University, 18 Ung Van Khiem St., Dong Xuyen Ward, Long Xuyen City, An Giang Province, Vietnam.
[2]Vietnam National University Ho Chi Minh City, Linh Trung Ward, Thu Duc City, Ho Chi Minh City, Vietnam.
[3]Department of Environmental Engineering, International University, Quarter 6, Linh Trung Ward, Thu Duc City, Ho Chi Minh City, Vietnam.
[4]Faculty of Environment and Natural Resources, Ho Chi Minh City University of Technology (HCMUT), 268 Ly Thuong Kiet St., Dist. 10, Ho Chi Minh City, Vietnam.

Received: 7th January 2022; Revised: 13th March 2022; Accepted: 14th March 2022
Available online: 21st March 2022; Published regularly: June 2022

Abstract

In this study, a facile low-temperature hydrothermal method was applied for the synthesis of bismuth subcarbonate nanoplates ($Bi_2O_2CO_3$). The material was then characterized by FTIR, XRD, SEM, BET, and TGA. The applicability of $Bi_2O_2CO_3$ was evaluated via the treatment of methyl blue (MB) in water by adsorption and photocatalytic degradation. The experiment results with different pH from 2 to 12 indicate that the pH of the solution affected the surface charge of the synthesized $Bi_2O_2CO_3$, thus having strong effects on the adsorption and photocatalytic degradation abilities of $Bi_2O_2CO_3$ for MB removal. In adsorption tests, pH 6–7 is the most suitable condition for the adsorption of $Bi_2O_2CO_3$. In photocatalytic tests, $Bi_2O_2CO_3$ had the highest and lowest efficiencies of 64.19% (pH 5) and 17.59% (pH 2), respectively, under UV irradiation for 300 min.

Keywords: $Bi_2O_2CO_3$; pH; Methylene Blue; Adsorption; Photocatalysis

How to Cite: T.T. Nguyen, T.T. Le, T.B.T. Nguyen, T.N. Thi, L.B. Tran, T.Q.A. Nguyen, N.H. Nguyen (2022). Effect of pH on the Performance of $Bi_2O_2CO_3$ Nanoplates for Methylene Blue Removal in Water by Adsorption and Photocatalysis. *Bulletin of Chemical Reaction Engineering & Catalysis*, 17(2), 331-339 (doi:10.9767/bcrec.17.2.13370.331-339)

Permalink/DOI: https://doi.org/10.9767/bcrec.17.2.13370.331-339

1. Introduction

Industries, such as: textiles and dyeing, cosmetics, plastics, paints, printing, and tanning, usually produced large quantities of colored wastewater caused by persistent organic matters. The presence of these dye compounds in the aquatic environment hinders the penetration of light and affects aquatic animals and plants [1]. Furthermore, dyes are recalcitrant, colorants, stable, and even potentially carcinogenic and toxic [2]. Therefore, these wastewater and dye compounds are of concern and it is necessary to treat them before being discharged into the environment to protect the environment as well as human health.

Textile dyeing wastewater was treated by many different methods such as chemical oxidation, precipitation, biological activated sludge,

* Corresponding Author.
Email: ntthanh@agu.edu.vn (T.T. Nguyen);
nnhuy@hcmut.edu.vn (N.H. Nguyen);

filtration, ozonation, reverse osmosis, or catalysis to remove different pollutant types in wastewater [3]. Among them, photocatalysts are developed and increasingly used for practical applications in the treatment of air pollution and water pollution [4]. Some photocatalytic nanomaterials are capable of treating and degrading dyes, such as TiO_2 and its modified forms [5–8], ZnO [9–11], and β-Bi_2O_3/$Bi_2O_2CO_3$ [12]. Among them, the $Bi_2O_2CO_3$ emerges as a new and effective material for adsorption and photocatalytic application. Depending on the preparation method, nanomaterials have different physical, chemical, and photocatalytic properties [13]. Besides, the photocatalytic efficiency of the materials is affected by environmental conditions such as temperature, pH, concentration, exposure time, and light intensity [8]. In particular, the pH value greatly affects the treatment efficiency of a photocatalytic process because the ions to be treated will transform into different forms and the material properties are also affected when the pH changes [14]. However, there has not been a report about the pH effect on the abilities of adsorption and photocatalysis of MB using $Bi_2O_2CO_3$ nanoplates.

Therefore, this study aims to examine the effect of pH on the color treatment in textile dyeing wastewater using photocatalyst. Specifically, the ability to remove methyl blue in the solution at different pH levels using $Bi_2O_2CO_3$ material was evaluated via both adsorption and photocatalysis. The mechanisms for adsorption and photocatalytic degradation of MB using $Bi_2O_2CO_3$ material were also proposed.

2. Materials and Methods

2.1 Materials

Lab-grade chemicals such as bismuth nitrate pentahydrate ($Bi(NO_3)_3.5H_2O$), hydrochloric acid (HCl), sodium hydroxide (NaOH), cetyltrimethylammonium bromide (CTAB, $[(C_{16}H_{33})N(CH_3)_3]Br$), sodium carbonate ($Na_2CO_3$), nitric acid ($HNO_3$), and methylene blue (MB, $C_{16}H_{18}ClN_3S$) were from China. Potassium bromide (KBr) for FTIR analysis was from Germany. Deionized water used in the experiments was from a local water machine in the laboratory.

2.2 Synthesis and Characterization of $Bi_2O_2CO_3$ Materials

$Bi_2O_2CO_3$ nanomaterial was prepared by hydrothermal method [15]. Firstly, 4.85 g $Bi(NO_3)_3.5H_2O$ was added and stirred in 10 mL of HNO_3 solution in a beaker for 30 min. The solution was then dropped slowly into a 90 mL solution containing 8.45 g of Na_2CO_3 and 1 g of CTAB under continuous stirring conditions. After 10 min of stirring, the material was filtered and washed several times with deionized water and alcohol before being dried at 60 °C for 4 h to obtain the $Bi_2O_2CO_3$ powder.

The surface morphology and elemental composition of $Bi_2O_2CO_3$ were studied by scanning electron microscopy (SEM-EDX, JCM-7000, JEOL, Japan). The crystalline structure was determined by X-ray diffraction (XRD, AERIS, Malvern Panalytical, The Netherlands) while the surface chemistry was examined by Fourier transform infrared spectroscopy (FTIR, Alpha, Bruker, Germany). The thermal stability and phase transformation of $Bi_2O_2CO_3$ were investigated by thermogravimetric analysis (TGA, model Q500, TA Instruments, USA). The surface area was measured by the Brunauer-Emmett-Teller method (BET Sorptometer, model BET-202A, Porous Materials, USA). The ultraviolet-visible light (UV-Vis) absorption of the material was measured by using a spectrophotometer (Cary 5000, Agilent, USA) and the bandgap was determined following our previous study [16].

The experiment to determine the isoelectric point (point of zero charge, pHpzc) of $Bi_2O_2CO_3$ was carried out as follows: 0.2 g of $Bi_2O_2CO_3$ was added to 50 mL of 0.1 M KCl 0.01 N in ten plastic beakers. The initial pH value (pH_0) was adjusted to 2–11 by 0.1 M HCl and 0.1 M NaOH and controlled by using a pH meter (Lab 850, SI Analytics, Germany). These solutions were shaken for 24 h and then measured the final pH value (pH_f). The isoelectric point of a material is the pH value that does not change or change very little from the initial value of the KCl solution. A graph showing the dependence of the difference between the initial and final pH values ($\Delta pH = pH_0 - pH_f$) on pH_0 was plotted and the point of intersection with the horizontal axis gives us the pHpzc value to be determined [17].

2.3 Adsorption and Photocatalysis Experiments

In adsorption tests, MB solutions with a volume of 50 mL and concentration of 20 mg/L were prepared and adjusted at different pH values using 0.1 M NaOH or 0.1 M HCl solutions. After that, 30 mg of $Bi_2O_2CO_3$ was added into the solution under magnetic stirring and let in the dark condition for 60 min of adsorption. The mixture was then centrifuged and the supernatant was taken for dye concentration

measurement a maximum absorbance peak of λ_{max} = 664 nm [18]. Ultraviolet and visible spectroscopy methods were used to determine the content of dyes in aqueous solutions and were performed on a UV–Vis spectrometer recorded on a SPECORD 210 UV-Visible Spectrophotometer (SPECORD 210, Analytik Jena, Germany). The solid material and the supernatant were then added back into the beaker and stirred in the dark condition for further photocatalytic tests. The UV light (7 W, λ = 350 nm) was then turned on for photocatalytic degradation of dye in the solution under continuous stirring and the MB concentration was measured at every 30 min of reaction.

The concentrations before and after degradation of MB were determined according to the equation:

$$C = 6.98 \times Abs - 1.11 \quad (1)$$

where, *Abs* is the absorbance of MB at the wavelength of λ_{max} = 664 nm and *C* is the concentration of MB. The photocatalytic degradation efficiency (η%) is calculated as follows:

$$\eta\% = \frac{C_0 - C_t}{C_0} \times 100 \quad (2)$$

where, C_0 is the initial MB concentration and C_t is the concentration after UV light irradiation.

3. Results and Discussion

3.1 Characterization of $Bi_2O_2CO_3$

As displayed in Figure 1(a) and 1(b), the synthesized $Bi_2O_2CO_3$ material consists of many flowerlike hierarchical microspheres with many petals fused together, which is similar to the study of Huang *et al.* [19]. SEM images with higher magnification in Figure 1(c) and 1(d) provide more detailed information about the microstructure, showing more porosity between them. This results in a high surface area of 38.3 m^2/g (BET result) for both adsorption and photocatalysis. As the surface area is larger and a more porous structure is present, the inner space of the hierarchical structures is more useful and facilitates the contact and interaction with the pollutants. The material $Bi_2O_2CO_3$ synthesized in this study has a larger surface area than $Bi_2O_2CO_3$ flower (24.43 m^2/g [20]) and $Bi_2O_2CO_3$ nanomaterial (33.2 m^2/g [21]) (Table 1). The large surface area of the material is also a favorable condition for light absorption, increasing the efficiency of the photocatalysis process to decompose the pollutants. The EDX result in Figure 2(a) shows an elemental composition of C, O, Al, and Bi with weight ratios of 24.2, 22.8, 4.2, and 48.8%, respectively, where Bi accounts for nearly 50%.

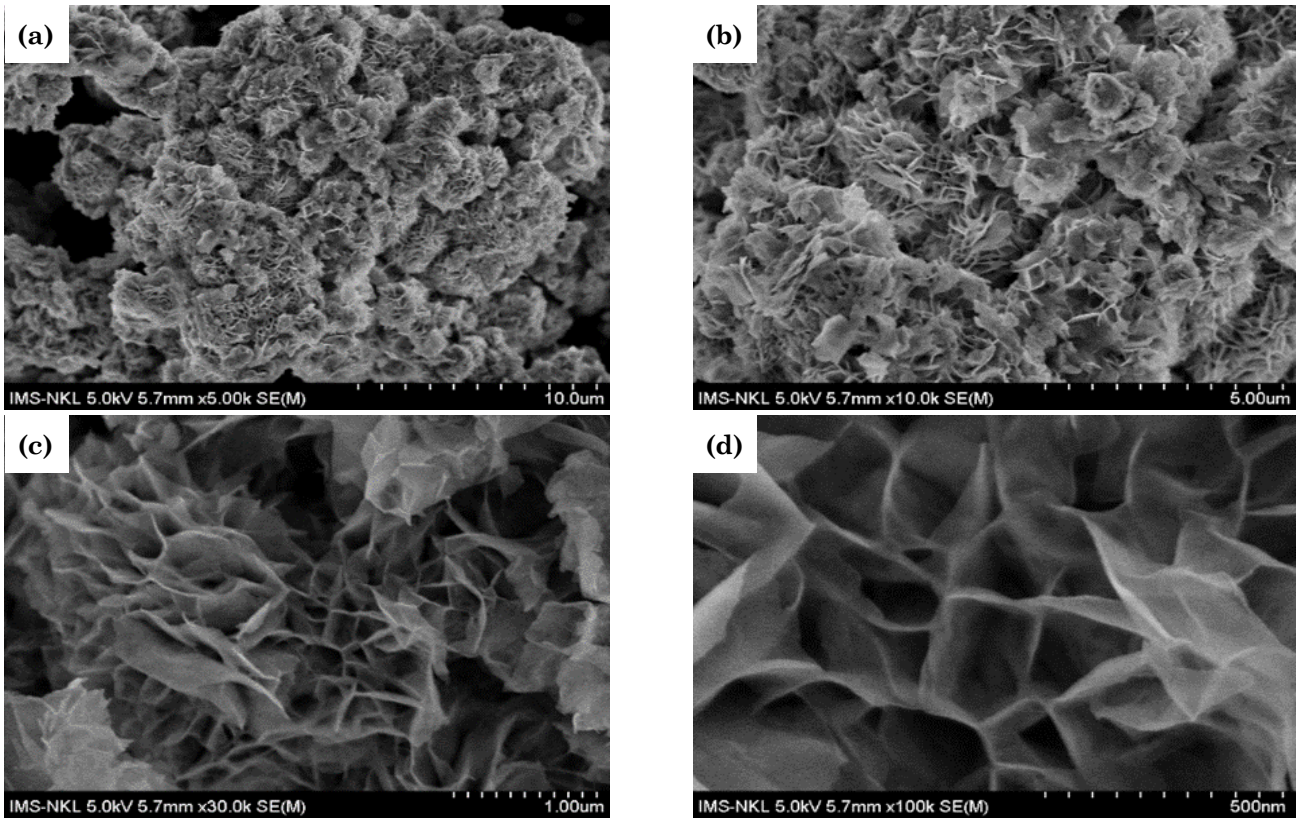

Figure 1. SEM images of synthesized $Bi_2O_2CO_3$ with different resolutions: (a) 5000x, (b) 10000x, (c) 30000x, and (d) 100000x magnification

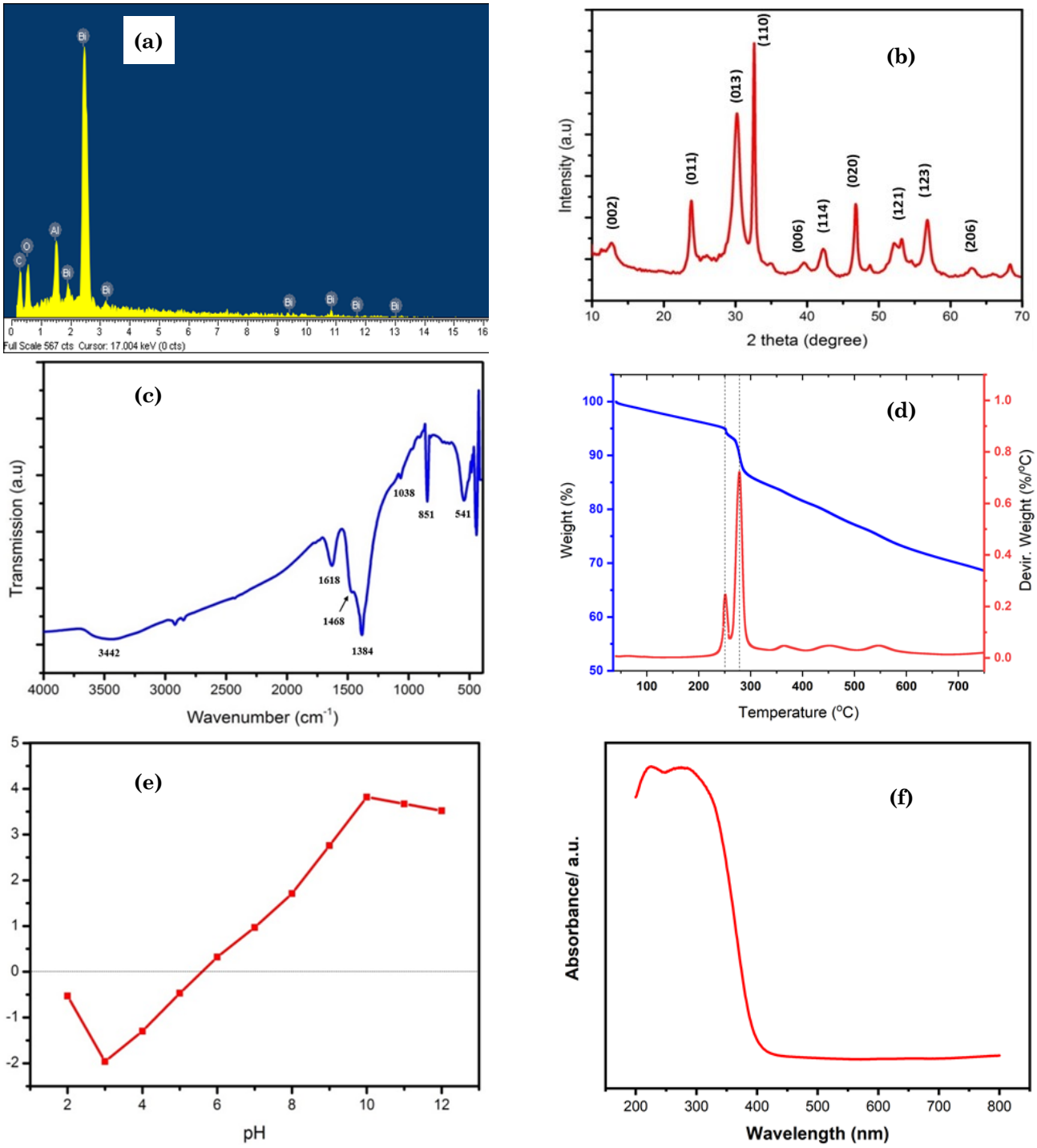

Figure 2. (a) EDX, (b) XRD, (c) FTIR, (d) TGA, (e) pHzpc, and (f) UV-Vis absorption results of the synthesized $Bi_2O_2CO_3$.

Table 1. Comparison of BET and XRD results with previous publications.

Material	BET (m^2/g)	Crystallite size (nm)	Reference
Flower-like $Bi_2O_2CO_3$	20.43	-	[20]
Sponge-like porous sphere $Bi_2O_2CO_3$	50.60	-	[20]
Plate-like $Bi_2O_2CO_3$	4.30	-	[20]
Sponge-like $Bi_2O_2CO_3$	33.2	-	[21]
Egg-tart shaped $Bi_2O_2CO_3$	40.8	-	[21]
Microspheres	22.86	30.2	[30]
Grinded microspheres	17.27	21.4	[30]
$Bi_2O_2CO_3$ microspheres	38.3	11.08	This study

As plotted in Figure 2(b), the XRD spectrum of the sample shows the appearance of a peak at 13.6°, 24.9°, 29.1°, 33.6°, 39.6°, 42.3°, 47.0°, 54.1°, 57.0°, and 63.1°, corresponding to planes of (002), (011), (013), (110), (006), (114), (020), (121), (123), and (206) (JCPDS Card No. 41-1488). The narrow peaks with high intensity at (013) and (110) are characteristic peaks of $Bi_2O_2CO_3$, showing that the photocatalytic material is successfully synthesized with good crystallinity. Moreover, the peak at (110) has a higher intensity than that at (013), indicating the anisotropic crystal growth along the (110) plane of the $Bi_2O_2CO_3$ flower-like microspheres [22]. The average crystal size calculated by the Debye-Scherrer equation from the (110) plane is 11.08 nm [23] and the comparison with other $Bi_2O_2CO_3$ is also provided in Table 1.

In the FTIR spectrum (Figure 2(c)), the peak at 541 cm^{-1} of the ionic carbonate is the characteristic peak of $Bi_2O_2CO_3$ nanomaterial. The peaks at 1384 and 1468 cm^{-1} are the stretching vibrations of C=O [19]. The bands at 541 and 851 cm^{-1} were assigned to the stretching vibration of Bi–O [24], while the wide band at 3442 cm^{-1} and peak at 1640 cm^{-1} are the stretching and deformation vibrations of OH^- groups in physically absorbed water molecules [25]. Overall, the results showed that no impurities (*e.g.* NO_3^-) were detected, which could confirm the purity of $Bi_2O_2CO_3$ nanomaterial.

Figure 2(d) shows the thermal stability, phase transformation, and composition change of $Bi_2O_2CO_3$ from 35 to 750 °C with a mass loss of 32%. There was a lightly loss in the mass of the sample at about 5% in the temperature range of 35–200 °C due to dehydration (*e.g.* moisture release). From 250 to 300 °C, the mass of $Bi_2O_2CO_3$ changed significantly with a mass loss of 9.5%, corresponding to the transformation reaction of $Bi_2O_2CO_3 \rightarrow Bi_2O_2 + CO_2$ [26].

The isoelectric point of $Bi_2O_2CO_3$ (pHpzc) was determined at 5.5 (Figure 2(e)) and it is an important parameter to determine the surface charge of the material under different solution pH. The UV-Vis absorption of the $Bi_2O_2CO_3$ material is presented in Figure 2(f), showing

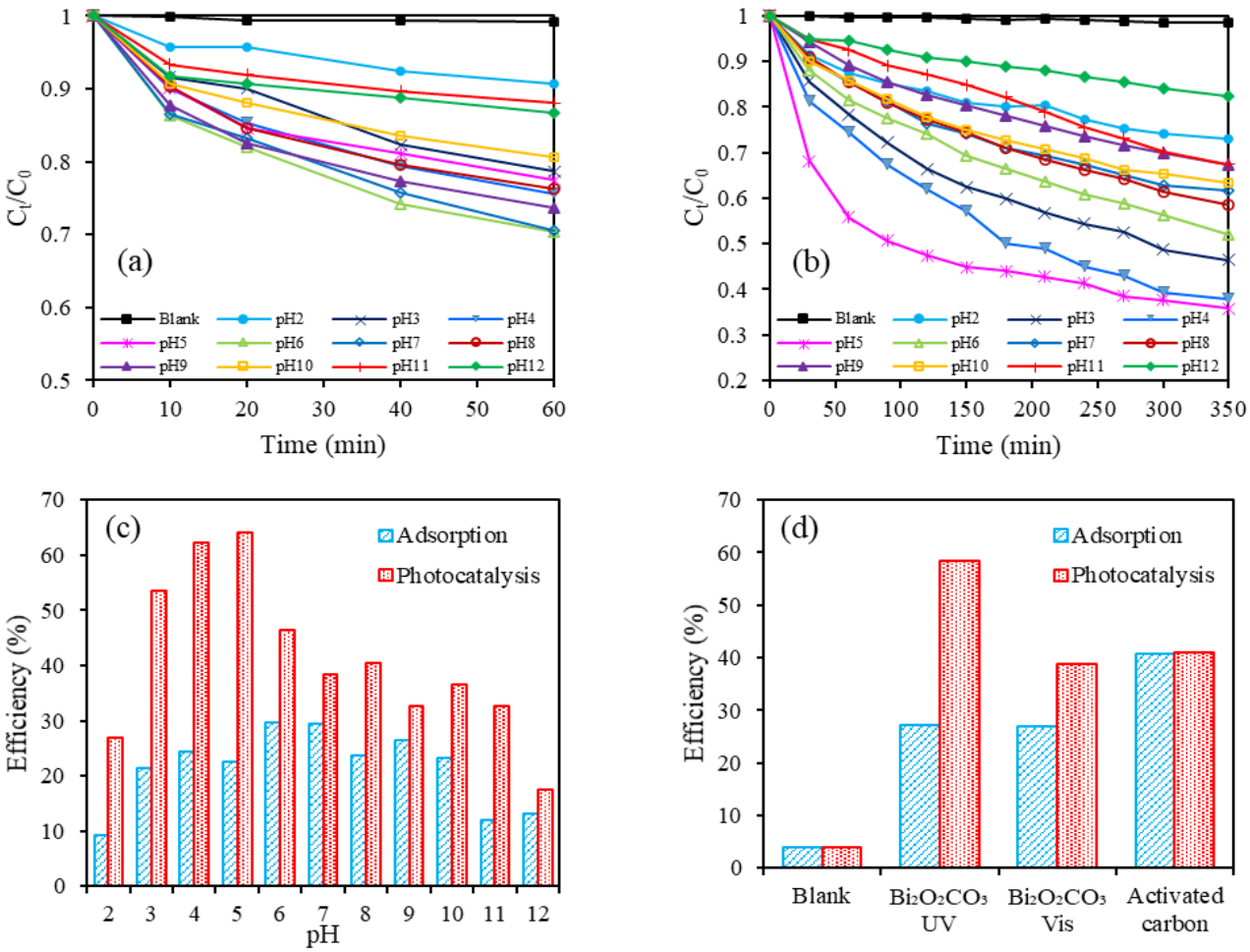

Figure 3. MB removal by (a) adsorption and (b) photocatalysis and the comparison of (c) pH effect on adsorption and photocatalysis and (d) effect of different processes.

that $Bi_2O_2CO_3$ is a good photocatalytic material in both UV and visible light irradiation with a calculated bandgap of 3.0 eV [16].

3.2 Adsorption of MB onto $Bi_2O_2CO_3$ Material

The adsorption of MB onto $Bi_2O_2CO_3$ is affected by the pH value of the MB solution, as demonstrated in Figure 3(a). The solution at pH 6 and pH 7 has higher adsorption capacities than those at the remaining pH values. Since the isoelectric point of $Bi_2O_2CO_3$ (pHpzc) was determined at 5. At pH <5.5, the positively charged surface of the material reduces its interaction with MB cations, resulting in low adsorption efficiency at pH ranges below 5 and especially the lowest efficiency at pH 2. This could also be because of the competition of H^+ ions with MB cations in solution from pH adjustment with HCl. When pH >5.5, the negatively charged surface of the material supports its interaction with MB cations, so the efficiency increases significantly. But when the pH value is too high (*e.g.*, pH 11 and 12), the excess of OH^- anion inhibits the interaction between the material surface and MB. In brief, the solution pH greatly affects the MB adsorption capacity of $Bi_2O_2CO_3$ material.

The MB degradation by photocatalysis using $Bi_2O_2CO_3$ during 6 h at different pH values is presented in Figure 3(b). The Langmuir-Hinshelwood kinetic was applied to describe the photocatalytic degradation of MB [27,28] with k (1/min) being the pseudo-first-order rate constant. Table 1 lists the pseudo-first-order rate constant determined from the slope of a plot of $\ln(C_0/C_t)$ versus t.

$$\ln\left(\frac{C_0}{C_t}\right) = kt \qquad (3)$$

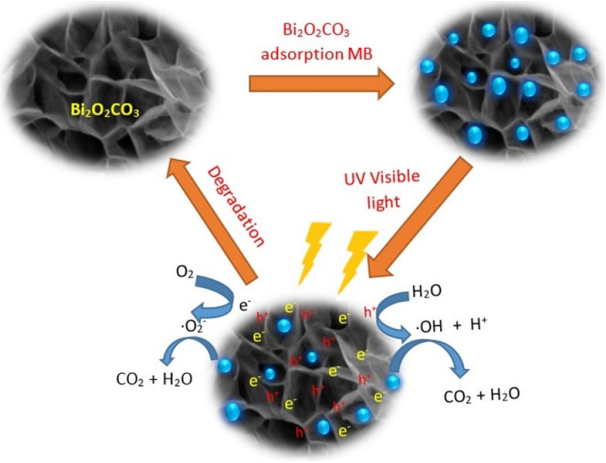

Figure 4. Proposed mechanism of MB adsorption and photocatalytic degradation using $Bi_2O_2CO_3$.

As compared in Figure 3(c), the degradation of MB by $Bi_2O_2CO_3$ reached the highest efficiency at pH 5. The rate of photocatalytic degradation k at different pH ranges was significantly different, of which the highest at pH 4 was 2.6×10^{-3} min^{-1} (Table 1). The results in Table 2 and Figure 3(c) showed that the MB adsorption efficiency at neutral pH was better than those at other pH values. In addition, acidic solutions are more effective than alkaline solutions for photocatalytic decomposition, which can be explained by the H^+ ion generated from photocatalysis, as illustrated in Equation (6) and Figure 4. With a large surface area and high pore volume, the adsorption sites inside or on the surface of the material are available to adsorb dye molecules in the solution. Once excited by ultraviolet light, electron-hole pairs are formed when electrons (e^-) are excited and enter the conduction band, leaving holes (h^+) in the valence band (Equation (4)). The photoexcited electrons and holes then migrate onto the $Bi_2O_2CO_3$ surface, where e^- reduces oxygen to form oxygen radicals ($^*O_2^-$, Equation (5)) while h^+ oxidizes water to form hydroxyl radicals ($^*OH$, Equation (6)), which then effectively degrade the MB in water (Equations (7) and (8)).

$$Bi_2O_2CO_3 + hv \rightarrow h^+ + e^- \qquad (4)$$
$$O_2 + e^- \rightarrow {}^*O_2^- \qquad (5)$$
$$H_2O + h^+ \rightarrow {}^*OH + H^+ \qquad (6)$$
$$MB + {}^*O_2^- \rightarrow CO_2 + H_2O \qquad (7)$$
$$MB + {}^*OH \rightarrow CO_2 + H_2O \qquad (8)$$

The comparisons of the MB removal efficiency by adsorption (by $Bi_2O_2CO_3$ and activated carbon) and photocatalysis under light irradiation (visible light and UV light) are shown in Figure 3(d). Results showed that $Bi_2O_2CO_3$ material has a lower MB adsorption efficiency

Table 2. Rate constants for photocatalytic degradation of MB using $Bi_2O_2CO_3$.

pH	k (10^{-3}/min)	R^2
2	0.7	0.9750
3	1.9	0.9835
4	2.6	0.9875
5	1.8	0.9071
6	1.6	0.9928
7	1.3	0.9801
8	1.4	0.9915
9	1.1	0.9897
10	1.1	0.9833
11	1.1	0.9933
12	0.5	0.9922

than activated carbon (*i.e.* 30% *vs.* 40%). However, after a period of exposure to light, the MB removal efficiency by activated carbon remained unchanged, while that by $Bi_2O_2CO_3$ increased significantly. Moreover, the efficiency increased by about 40% under visible light and about 60% under UV light. The adsorption capacity of activated carbon was higher because it has a large surface area of about 180.5 m^2/g [29] as compared to 38.3 m^2/g for $Bi_2O_2CO_3$. The photocatalytic removal of MB under UV light was higher than that of visible light. This can be explained by the bandgap of the $Bi_2O_2CO_3$ is 3.0 eV, thus it can not effectively utilize the whole range of visible light for the photocatalytic process.

The effects of solution temperature and initial MB concentration on its photocatalytic removal are shown in Figure 5. As seen in Figure 5(a), the MB removal efficiency is proportional to the temperature. The treatment efficiency at 40 °C was quite high at more than 75% while those at 20 and 30 °C were only around 55%. This is possible because the intrinsic photocatalytic reaction rate increases at a higher temperature, and also the molecules of MB become more mobile, facilitating the ability to contact with $Bi_2O_2CO_3$ surface. As seen in Figure 5(b), the MB decomposition efficiency was inversely proportional to the increase in MB concentration. This may be because the increased concentration of MB corresponds to the increase in color in the water, thereby affecting the transmission of light to the surface of $Bi_2O_2CO_3$ material. Also, more MB needs more hydroxyl radicals for the degradation. Also, under a fixed amount of $Bi_2O_2CO_3$ and light intensity, more MB needs more time to be degraded. It can be seen that the MB removal efficiency decreases nearly halved from more than 80% to about 40% when the MB concentration increased from 5 to 30 mg/L.

4. Conclusions

This study successfully synthesized and characterized $Bi_2O_2CO_3$ photocatalyst material by facile hydrothermal method. In the MB removal test, the solution pH had a great influence on the adsorption capacity as well as the photocatalytic removal efficiency. The adsorption was highest at pH 6 and 7 with the adsorption efficiency of more than 29.7% after 60 min while the photocatalytic degradation was highest at pH 5 with an efficiency of 64.19% under UV light after 300 min.

References

[1] Afkhami, A., Saber-Tehrani, M., Bagheri, H. (2010). Modified maghemite nanoparticles as an efficient adsorbent for removing some cationic dyes from aqueous solution. *Desalination*, 263, 240–248. DOI: 10.1016/j.desal.2010.06.065

[2] Gonawala, K.H., Mehta, M.J. (2014). Removal of color from different dye wastewater by using ferric oxide as an adsorbent. *International Journal of Engineering Research and Applications,* 4, 102–109.

[3] Marimuthu, S., Antonisamy, A.J., Malayandi, S., Rajendran, K., Tsai, P.-C., Pugazhendhi, A., Ponnusamy, V.K. (2020). Silver nanoparticles in dye effluent treatment: A review on synthesis, treatment methods, mechanisms, photocatalytic degradation, toxic effects and mitigation of toxicity. *Journal of Photochemistry and Photobiology B: Biology,* 205, 111823. DOI: 10.1016/j.jphotobiol.2020.111823

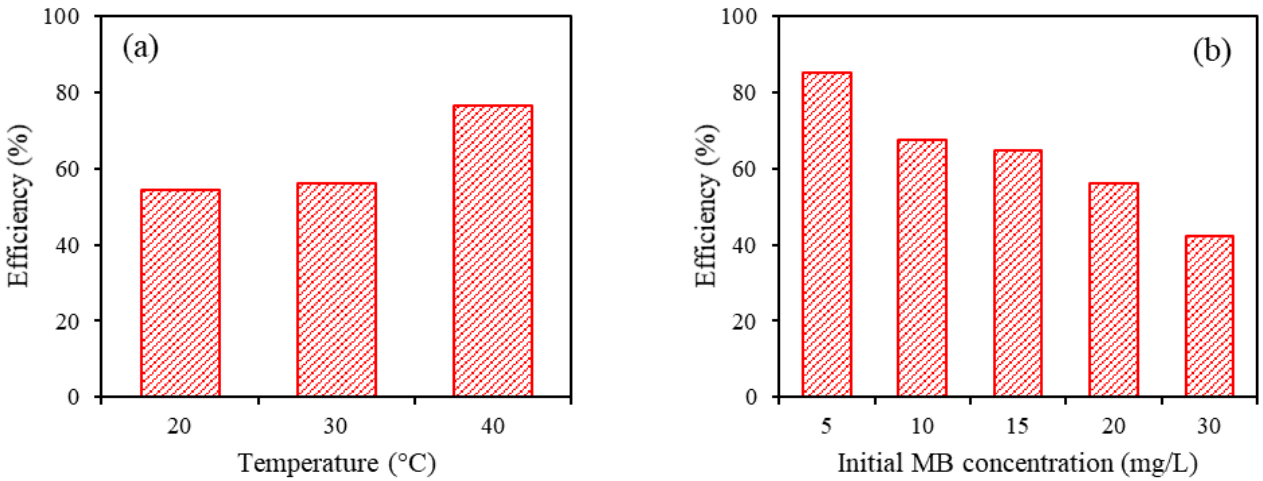

Figure 5. Effects of (a) solution temperature and (b) initial MB concentration on the photocatalytic removal of MB using $Bi_2O_2CO_3$.

[4] Payan, A., Fattahi, M., Roozbehani, B. (2018). Synthesis, characterization and evaluations of TiO_2 nanostructures prepared from different titania precursors for photocatalytic degradation of 4-chlorophenol in aqueous solution. *Journal of Environmental Health Science & Engineering,* 16, 41–54. DOI: 10.1007/s40201-018-0295-5

[5] Reddy, D.R., Dinesh, G.K., Anandan, S., Sivasankar, T. (2016). Sonophotocatalytic treatment of Naphthol Blue Black dye and real textile wastewater using synthesized Fe doped TiO_2. *Chemical Engineering and Processing: Process Intensification,* 99, 10–18. DOI: 10.1016/j.cep.2015.10.019

[6] Al-Mamun, M., Kader, S., Islam, M., Khan, M. (2019). Photocatalytic activity improvement and application of UV-TiO_2 photocatalysis in textile wastewater treatment: A review. *Journal of Environmental Chemical Engineering,* 7, 103248. DOI: 10.1016/j.jece.2019.103248

[7] Thi Khanh Van, N., Dinh, N.N., Van Chien, N., Huy, N.N., Trung, N.T., Toan, T.Q., *Van Thanh, D.* (2021). A simple and efficient ultrasonic-assisted electrochemical approach for scalable production of nitrogen-doped TiO_2 nanocrystals. *Nanotechnology,* 32, 465602. DOI: 10.1088/1361-6528/ac1b55

[8] Que, V.N.X., Khoi, T.T., Thuy, N.T., Dung, T.T.M., Binh, D.T.T., Huy, N.N. (2021). Factors Determining the Removal Efficiency of Procion MX in Waters Using Titanate Nanotubes Catalyzed by UV Irradiation. *Journal of Nanotechnology,* 2021, 8870453. DOI: 10.1155/2021/8870453

[9] Chakrabarti, S., Dutta, B.K. (2004). Photocatalytic degradation of model textile dyes in wastewater using ZnO as semiconductor catalyst. *Journal of Hazardous Materials,* 112, 269–278. DOI: 10.1016/j.jhazmat.2004.05.013

[10] Bagheri, M., Najafabadi, N.R., Borna, E. (2020). Removal of reactive blue 203 dye photocatalytic using ZnO nanoparticles stabilized on functionalized MWCNTs. *Journal of King Saud University-Science,* 32, 799–804. DOI: 10.1016/j.jksus.2019.02.012

[11] Weldegebrieal, W., Kassegn, G. (2020). Synthesis method, antibacterial and photocatalytic activity of ZnO nanoparticles for azo dyes in wastewater treatment: A review. *Inorganic Chemistry Communications,* 120, 108140. DOI: 10.1016/j.inoche.2020.108140

[12] Li, J.-h., Ren, J., Hao, Y.-j., Zhou, E.-p., Wang, Y., Wang, X.-j., Su, R., Liu, Y., Qi, X.-h., Li, F.-t. (2021). Construction of ß-Bi_2O_3/$Bi_2O_2CO_3$ heterojunction photocatalyst for deep understanding the importance of separation efficiency and valence band position. *Journal of Hazardous Materials,* 401, 123262. DOI: 10.1016/j.jhazmat.2020.123262

[13] Shahbazi, R., Payan, A., Fattahi, M. (2018). Preparation, evaluations and operating conditions optimization of nano TiO_2 over graphene based materials as the photocatalyst for degradation of phenol. *Journal of Photochemistry and Photobiology A: Chemistry,* 364, 564–576. DOI: 10.1016/j.jphotochem.2018.05.032

[14] Bedia, J., Muelas-Ramos, V., Peñas-Garzón, M., Gómez-Avilés, A., Rodríguez, J.J., Belver, C. (2018). A review of photocatalytic water purification with metal organic frameworks. *Catalysts,* 9, 52. DOI: 10.3390/catal9010052

[15] Chen, L., Huang, R., Yin, S.-F., Luo, S.-L., Au, C.-T. (2012). Flower-like $Bi_2O_2CO_3$: Facile synthesis and their photocatalytic application in treatment of dye-containing wastewater. *Chemical Engineering Journal,* 193, 123–130. DOI: 10.1016/j.cej.2012.04.023

[16] Nguyen, N.H., Wu, H.-Y., Bai, H. (2015). Photocatalytic reduction of NO_2 and CO_2 using molybdenum-doped titania nanotubes. *Chemical Engineering Journal,* 269, 60–66. DOI: 10.1016/j.cej.2015.01.099

[17] Kosmulski, M. (2006). pH-dependent surface charging and points of zero charge: III. Update. *Journal of Colloid Interface Science,* 298, 730–741. DOI: 10.1016/j.jcis.2006.01.003

[18] Van Hao, P., Minh, P.N., Hong, P.N., Huy, N.N., Oanh, P.T., Nguyen, H.T., Tran, T.D., Van Thanh, D., Van Dang, N. (2021). Gram-scale synthesis of electrochemically oxygenated graphene nanosheets for removal of methylene blue from aqueous solution. *Nanotechnology,* 32, 16LT01. DOI: 10.1088/1361-6528/abdc8b

[19] Huang, Y., Fan, W., Long, B., Li, H., Zhao, F., Liu, Z., Tong, Y., Ji, H. (2016). Visible light Bi_2S_3/Bi_2O_3/$Bi_2O_2CO_3$ photocatalyst for effective degradation of organic pollutions. *Applied Catalysis B: Environmental,* 185, 68–76. DOI: 10.1016/j.apcatb.2015.11.043

[20] Zheng, Y., Duan, F., Chen, M., Xie, Y. (2010). Synthetic $Bi_2O_2CO_3$ nanostructures: novel photocatalyst with controlled special surface exposed. *Journal of Molecular Catalysis A: Chemical,* 317, 34–40. DOI: 10.1016/j.molcata.2009.10.018

[21] Yang, L., Han, Q., Zhu, J., Wang, X. (2015). Synthesis of egg-tart shaped $Bi_2O_2CO_3$ hierarchical nanostructures from single precursor and its photocatalytic performance. *Materials Letters,* 138, 235–237. DOI: 10.1016/j.matlet.2014.10.003

[22] Cheng, H., Huang, B., Yang, K., Wang, Z., Qin, X., Zhang, X., Dai, Y. (2010). Facile template-free synthesis of $Bi_2O_2CO_3$ hierarchical microflowers and their associated photocatalytic activity. *ChemPhysChem,* 11, 2167–2173. DOI: 10.1002/cphc.200901017

[23] Nguyen, N.H., Bai, H. (2014). Photocatalytic removal of NO and NO_2 using titania nanotubes synthesized by hydrothermal method. *Journal of Environmental Sciences,* 26, 1180–1187. DOI: 10.1016/S1001-0742(13)60544-6

[24] Wang, B., Wang, J., Zhang, Y., Mei, Y., Lian, P. (2017). Electrochemical performance of $Bi_2O_2CO_3$ nanosheets as negative electrode material for supercapacitors. *Ceramics International,* 43, 9310–9316. DOI: 10.1016/j.ceramint.2017.04.092

[25] Nguyen, T.T., Le, T.T., Phan, P.T., Nguyen, N.H. (2020). Preparation, characterization, and application of novel ferric oxide-amine material for removal of nitrate and phosphate in water. *Journal of Chemistry,* 2020, 8583543. DOI: 10.1155/2020/8583543

[26] Yu, C., Zhou, W., Zhu, L., Li, G., Yang, K., Jin, R. (2016). Integrating plasmonic Au nanorods with dendritic like α-Bi_2O_3/$Bi_2O_2CO_3$ heterostructures for superior visible-light-driven photocatalysis. *Applied Catalysis B: Environmental,* 184, 1–11. DOI: 10.1016/j.apcatb.2015.11.026

[27] Asenjo, N.G., Santamaria, R., Blanco, C., Granda, M., Alvarez, P., Menendez, R. (2013). Correct use of the Langmuir–Hinshelwood equation for proving the absence of a synergy effect in the photocatalytic degradation of phenol on a suspended mixture of titania and activated carbon. *Carbon,* 55, 62–69. DOI: 10.1016/j.carbon.2012.12.010

[28] Kumar, K.V., Porkodi, K., Rocha, F. (2008). Langmuir–Hinshelwood kinetics–a theoretical study. *Catalysis Communications,* 9, 82–84. DOI: 10.1016/j.catcom.2007.05.019

[29] Sharma, Y.C. (2010). Optimization of parameters for adsorption of methylene blue on a low-cost activated carbon. *Journal of Chemical Engineering Data,* 55, 435–439. DOI: 10.1021/je900408a

[30] Madhusudan, P., Zhang, J., Cheng, B., Liu, G. (2013). Photocatalytic degradation of organic dyes with hierarchical $Bi_2O_2CO_3$ microstructures under visible-light. *CrystEngComm,* 15, 231–240. DOI: 10.1039/C2CE26639C